Nanoscale

PAPER

View Article Online
View Journal | View Issue

Cite this: *Nanoscale*, 2023, **15**, 5403

Programming rigidity into size-defined wireframe DNA nanotubes†

Daniel Saliba,‡[a] Xin Luo, ‡[a] Felix J. Rizzuto [a,b] and Hanadi F. Sleiman *[a]

Nanotubes built from DNA hold promise for several biological and materials applications, due to their high aspect ratio and encapsulation potential. A particularly appealing goal is to control the size, shape, and dynamic behaviour of DNA nanotubes with minimal design alteration, as nanostructures of varying morphologies and lengths have been shown to exhibit distinct cellular uptake, encapsulation behaviour, and *in vivo* biodistribution. Herein, we report a systematic investigation, combining experimental and computational design, to modulate the length, flexibility, and longitudinal patterns of wireframe DNA nanotubes. Subtle design changes govern the structure and properties of our nanotubes, which are built from a custom-made, long, and size-defined template strand to which DNA rungs and linkers are attached. Unlike DNA origami, these custom-made strands possess regions with repeating sequences at strategic locations, thereby reducing the number of strands necessary for assembly. Through strand displacement, the nanotubes can be reversibly altered between extended and collapsed morphologies. These design concepts enable fine-tuning of the nanotube stiffness and may pave the way for the development of designer nanotubes for a variety of applications, including the study of cellular internalization, biodistribution, and uptake mechanisms for structures of varied shapes and sizes.

Received 4th November 2022,
Accepted 11th February 2023

DOI: 10.1039/d2nr06185f

rsc.li/nanoscale

Introduction

The controlled self-assembly of discrete DNA nanostructures with well-defined geometries and narrow size distribution has received considerable attention for applications in advanced electronics, nanooptics, and nanomedicine.[1–4] DNA nanotubes are especially promising in this respect, due to their high aspect ratio, shape persistence, and continuous nanoscale cavities, allowing their use as bioreactors,[5,6] transmembrane channels,[7] and drug delivery vehicles.[8–10] The external scaffold of DNA nanotubes possesses numerous ordered binding sites that can be used as templates to guide the precise assembly of other functional components along the tubes, including nanoparticles,[11,12] fluorescent dyes,[13] and proteins.[14]

Prominent methods to synthesize DNA nanotubes, tile-based assembly and DNA origami,[15–17] have produced a range of cavity sizes and tube lengths but nevertheless have inherent limitations: nanotube length is uncontrolled when constructed with DNA tiles, which can furthermore propagate curvature and defects from the main tile building block;[18–23] the level of structural complexity achieved by DNA origami comes at the expense of using hundreds of unique staple strands and is limited by the size of the viral DNA scaffold; moreover, both structures require the use of magnesium concentrations that are significantly higher than in physiological conditions.[24–27]

Alternatively, our group has reported a modular nanotube assembly method based on prefabricated DNA rungs and DNA linkers, showing their use as dynamic scaffolds for the organization of plasmonic nanoparticles and as vehicles for drug delivery.[9,28–31] These wireframe DNA assemblies often produce a wide range of tube lengths or else rely on DNA building blocks with synthetic vertices, limiting their scalable production.[32–34] A size-defined template strand circumnavigated these issues, generating a monodisperse nanotube; however, the inherent flexibility of this design led to collapsed structures with low persistence length.[35]

Modularity in nanotube design could be used to retain guest molecules with differing levels of exposure to the external environment; different mechanisms of cell entry can be engineered by forming length-, shape-, and density-specific architectures. For example, it has been demonstrated that a DNA tetrahedron penetrates the cell *via* a "corner-attack" mechanism that avoids contact with the cytoplasmic membrane.[36,37] Additionally, DNA origami nanostructures with rectangular, triangular, or tubular geometries demonstrated different *in vivo* activities in renal disease treatment.[38] Ordered binding sites along the external scaffold of these con-

[a]*Department of Chemistry, McGill University, 801 Sherbrooke St. West, Montreal, QC, H3A 0B8, Canada. E-mail: hanadi.sleiman@mcgill.ca*
[b]*School of Chemistry, University of New South Wales, Sydney, 2052, Australia*
†Electronic supplementary information (ESI) available. See DOI: https://doi.org/10.1039/d2nr06185f
‡These authors contributed equally.

structs can template the assembly of functional components (including nanoparticles,[11,12] fluorescent dyes,[13] and proteins[14]) with nanoscale precision, but it is the morphology of the nanotube – its rigidity, cavity size, and persistence length – that often determines component proximity and hence function.[10] It is necessary to understand the construction parameters dictating the morphology of wireframe DNA nanotubes, how they assemble, and what factors govern their mechanical properties, to design nanomaterials with absolute spatial patterning.

Herein, we report a systematic study, incorporating experimental and computational design at the single-nucleotide level,[39–43] for modulating the flexibility of wireframe DNA nanotubes. Our DNA nanotubes are templated by long and size-defined template strands possessing regions with repeating sequences at strategic locations, thus minimizing the number of strands required for assembly. Relationships between the number of unpaired bases and the structure of building blocks are directly correlated to strain accumulated along the nanotube length, which in turn dictates nanotube integrity. By merging principles of DNA tile-based assembly with our wireframe constructs, we developed DNA nanotubes with controllable rigidity and length, well-defined rung placements, and periodic, structured cavities. Our structures are simple to prepare, require few DNA sequences, and have adaptable morphologies that may find broad use in delivery applications, such as how shape and size impact the biological properties and cellular internalization of DNA nanostructures.[44]

Results and discussion

Design parameters for size-defined DNA nanotubes

Our DNA nanotubes are composed of triangular rungs held together by linking strands (LSs) and a long pillar strand (PS) (*e.g.*, Fig. 1(B)). When organizing functional molecules on a DNA scaffold (*e.g.*, DNA origami), a large portion of the scaffold usually serves a purely structural role, providing rigidity and orientation. Only a small number of specific positions need to be addressable to attach cargo. As such, it is practical to build scaffolds in which the addressable sites are positioned selectively within a framework of identical, repeating structural motifs, allowing the construct to be built from significantly fewer components rather than the hundreds of strands required for DNA origami. Our DNA pillar strand is created by a rapid and practical method that takes approximately two days, starting from a handful of commercially available building blocks.[35] Once the strand is created, it can be PCR amplified and re-used in multiple constructs. One of the main strengths of our temporal growth approach is the ability to combine quickly and easily symmetric, repeating sequence domains with asymmetric, unique ones in virtually any arrangement. Another notable advantage of temporal growth over DNA origami is that the size of the DNA object can be significantly larger, as the structure is not constrained by the folding of a viral scaffold strand. This approach allows the modification of any repeating unit down the nanotube length independently from the others and can result in unique addressable sites along the nanotube. The resulting template strand has alternating, repeating domains: R′ (Fig. 1(A), orange domain), which contains 42 base pairs onto which the rung units hybridize, and LS′ (Fig. 1(A), blue domain), which has 21 base pairs and forms one of the edges of the nanotube's cavity.

All triangular rung units are appended with single-stranded binding regions at one corner and sticky-ends that allow binding to the linking strands at the remaining two. To inhibit intermolecular crosslinking between nanotubes and favor the formation of discrete structures, we modified the design of the rung units that hybridize to the 5′ and 3′ termini of the PS template. For the top rung, the three overhangs above the plane were removed (leaving the 2 sticky-ends below the plane intact), whereas the three overhangs below the plane of the bottom rung were removed (keeping 2 sticky-ends above the plane) (*e.g.* Fig. 1(B)). Combining these rung units with the PS scaffold results in an open-form nanotube. The subsequent addition of linking strands results in the formation of a fully closed triangular nanotube.

Three distinct types of rung units were used, resulting in nanotubes with varying degrees of flexibility: (i) type I rungs, consisting of a linear strand that folds into a triangular shape (Fig. 1(B)); (ii) type II rungs, comprising of a circular strand onto which the rung components hybridize (Fig. 1(C)); and (iii) and type III rungs, composed of a circularized strand and DX-tile linkage onto the PS template (Fig. 1(D)).

NT_1 – a size-defined DNA nanotube with a collapsed morphology

The self-assembly of our first-generation nanotube (NT_1) was achieved by firstly hybridizing type I rung units (Fig. 2(A) – composed of five unmodified, linear DNA strands[32,34,35]) to the pillar strand, followed by the hybridization of linking strands LS1/LS1′ and LS2/LS2′, generating a fully double-stranded construct. Agarose gel electrophoresis (AGE) showed the formation of a non-penetrating and smeary band (Fig. 2 (A)), consistent with a large, highly disperse structure, unlike the expected single band that would indicate the formation of a monodisperse product. Large aggregates were observed by AFM (Fig. 2(A) and ESI, Fig. S11(B)†), suggesting the formation of a collapsed, flexible nanotube that is potentially branched and self-polymerized.

We employed vHelix and oxDNA to build and perform MD simulations of these structures.[40,43] Simulations revealed an average twisting of 91° at the connection sites of the rungs to the pillar in ds-NT_1 (Fig. 2(A)), rather than a straight arrangement perpendicular to the triangular unit, as required for the formation of a closed nanotube. This high degree of twist at the rung corner suggests that the addition of the fully double-stranded linking strands leads to a greater likelihood of connecting to the units of a different nanotube, rather than the next rung unit of the same tube.

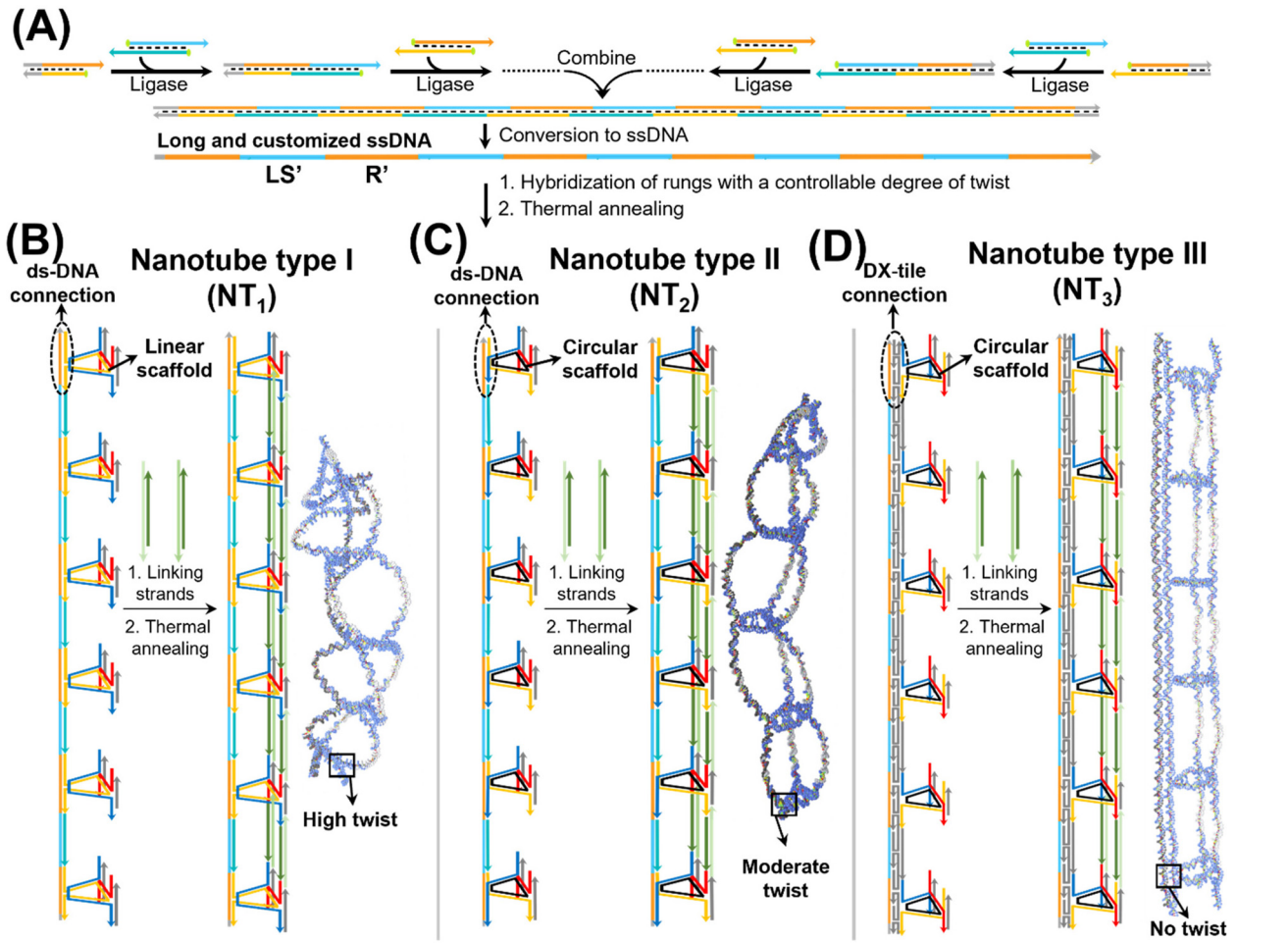

Fig. 1 Production of uniform and extended scaffold strands (PS) and assembly of periodic nanotube structures with a controllable degree of flexibility. The production of size-defined scaffold strands with repeating domains involves adding sticky-ended dsDNA building blocks sequentially in the desired order while *in situ* enzymatic ligation occurs. After PCR enrichment and enzymatic conversion to ssDNA, the final product is obtained (A). The pre-formed rung units hybridize with one of the repetitive domains, whilst the spacer strand hybridizes with the other. The addition of linking strands results in the formation of the nanotube. The design of the rung units results in nanotubes with a controllable degree of flexibility: (i) a rung unit with a high degree of twist results in a collapsed nanotube (NT_1) (B); (ii) a rung unit with a moderate degree of twist results in a partially extended nanotube (NT_2) (C); and (iii) a rung unit with no twist results in a rigid nanotube (NT_3) (D).

By deleting one base from the linking strands, we hypothesized that the additional flexibility would allow the LS to connect to an adjacent rung on the same tube, rather than crosslinking to other structures. AGE analysis demonstrated the production of a well-defined, monodisperse structure, and AFM showed collapsed partial ds-NT_1 with a high degree of flexibility (Fig. 2(B) and ESI, Fig. S12(B)†). MD simulations suggested that these ssDNA gaps proffered increased flexibility with an average twisting of 78° (Fig. 2(B)) at the connection sites of the rungs to the pillar, in comparison to an average twisting of 91° in the fully double-stranded predecessor; however, this strategy still resulted in a collapsed structure by AFM in air. The height profiles of each individual rung unit as determined by AFM were found to be approximately 1.5 nm; the collapsed structures range in height from 1.5 to 2.0 nm. This increase in height may imply that the rung units are stacked on top of one another on the mica surface, due to the high flexibility of the nanotube. Finally, using totally single-stranded linking strands produces nearly monodisperse products by AGE, and completely collapsed structures by AFM in air, with a height ranging from 1.8 to 2.3 nm (Fig. 2(C) and ESI, Fig. S13(B)†), implying that the rung units are also stacked on one another, as for the partial ds-NT_1 design.[45,46] Type I rung thus has a less-than-ideal angle of 180° between the top and bottom connecting strand arms. This angle is required to ensure that the linking strand arms are positioned linearly within the assembled nanotube. The angular tension in each rung unit accumulates in the nanotube structure, producing discrete yet collapsed structures.

NT_2 – a size-defined DNA nanotube with a flexible and extended morphology

To produce more rigid nanotubes, we employed a rung unit with reduced twist. This new rung incorporates a circular tem-

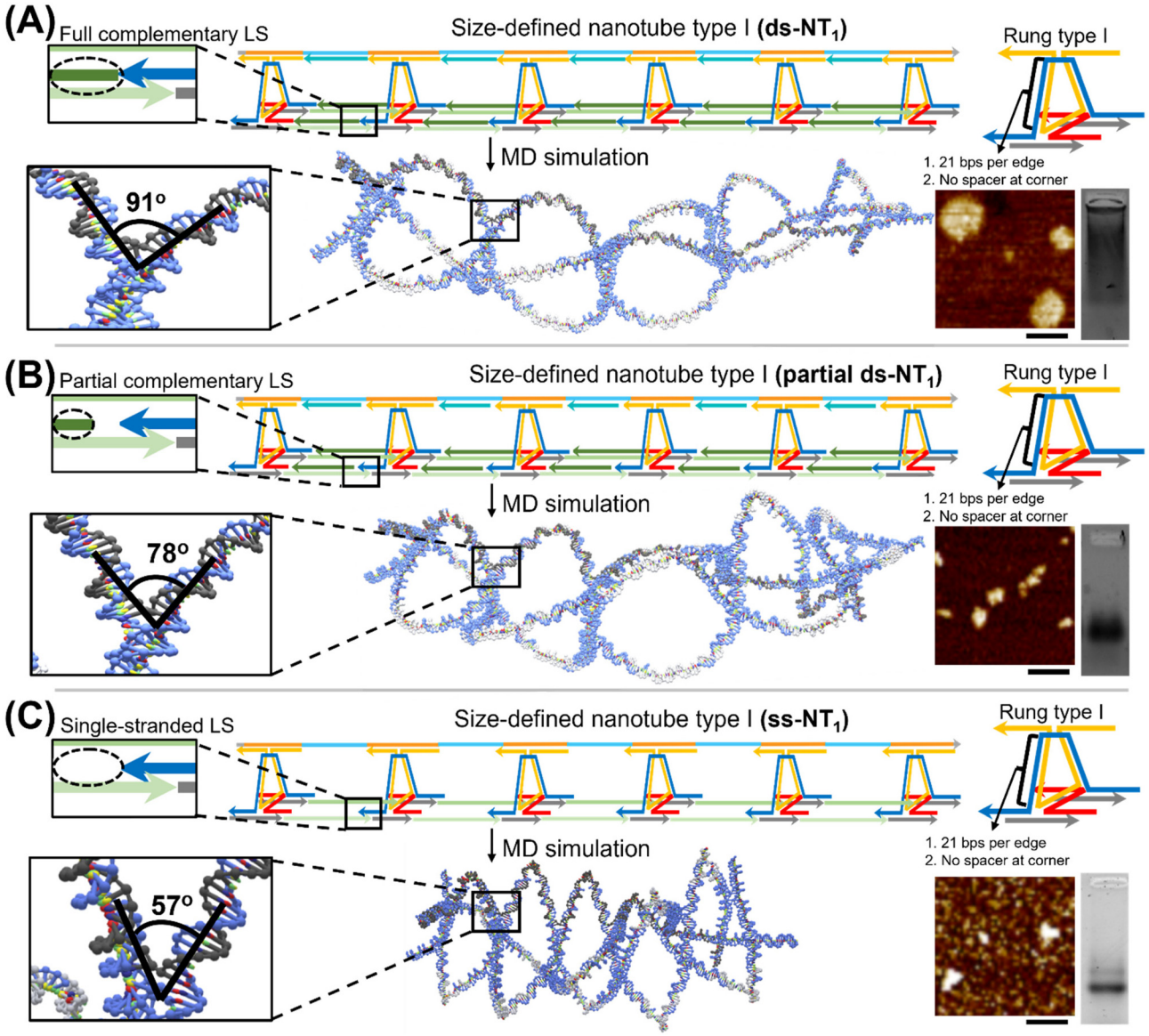

Fig. 2 Schematic representation of the fully double-stranded (ds-NT_1), partially double-stranded (partial ds-NT_1) and single-stranded (ss-NT_1) size-defined DNA nanotube type I. The triangular units are hybridized onto the pillar and the construction of the nanotube is completed by adding fully complementary linking strands (A), partially complementary linking strands (B) or single-stranded linking strands (C). MD simulations reveal a 91-degree, 78-degree and 57-degree angle between the rung overhangs below the triangular plane and those above the plane at the connection sites of the rungs to the pillar for ds-NT_1, partial ds-NT_1 and ss-NT_1, respectively. Aggregates are detected by AFM for the ds-NT_1, whereas partial ds-NT_1 and ss-NT_1 form collapsed structures. The scale bar is equal to 90 nm. Smearing is detected by AGE for ds-NT_1, whereas a major well-defined band is detected for partial ds-NT_1 and ss-NT_1.

plate onto which the component strands can hybridize (Fig. 3). Due to the helical twist of DNA at the rung corner, adding or removing a base pair at this position changes the angle of the twist between the helix ends, resulting in increased or decreased strain at the rung-to-pillar connection sites.

MD simulations revealed notable impacts of single-base pair alterations on the overall stiffness of the nanotube, reflected in the end-to-end distance between the first and last bases of the scaffold strand. The end-to-end distance in an ideal rigid nanotube is equal to the length of the fully stretched scaffold (115 nm), whereas shorter distances will be detected for nanotubes with increased flexibility as the degree of twist at the rung corner increases. The designs were iteratively optimized, investigating the effects of (i) the length of the rung edges, 20 bps per edge and 21 bps per edge, (ii) the presence or absence of a spacer on each of the circular template corners, and (iii) the use of a nicked or ligated circular core template. The length of the rung edge (20 bps or 21 bps) and the presence or absence of a corner spacer (2 thymine bases or no spacer) had a considerable influence on the nanotube assembly. Rung units consisting of 20 bases per edge and having 2-thymine bases as a spacer (type IIa) tended to form

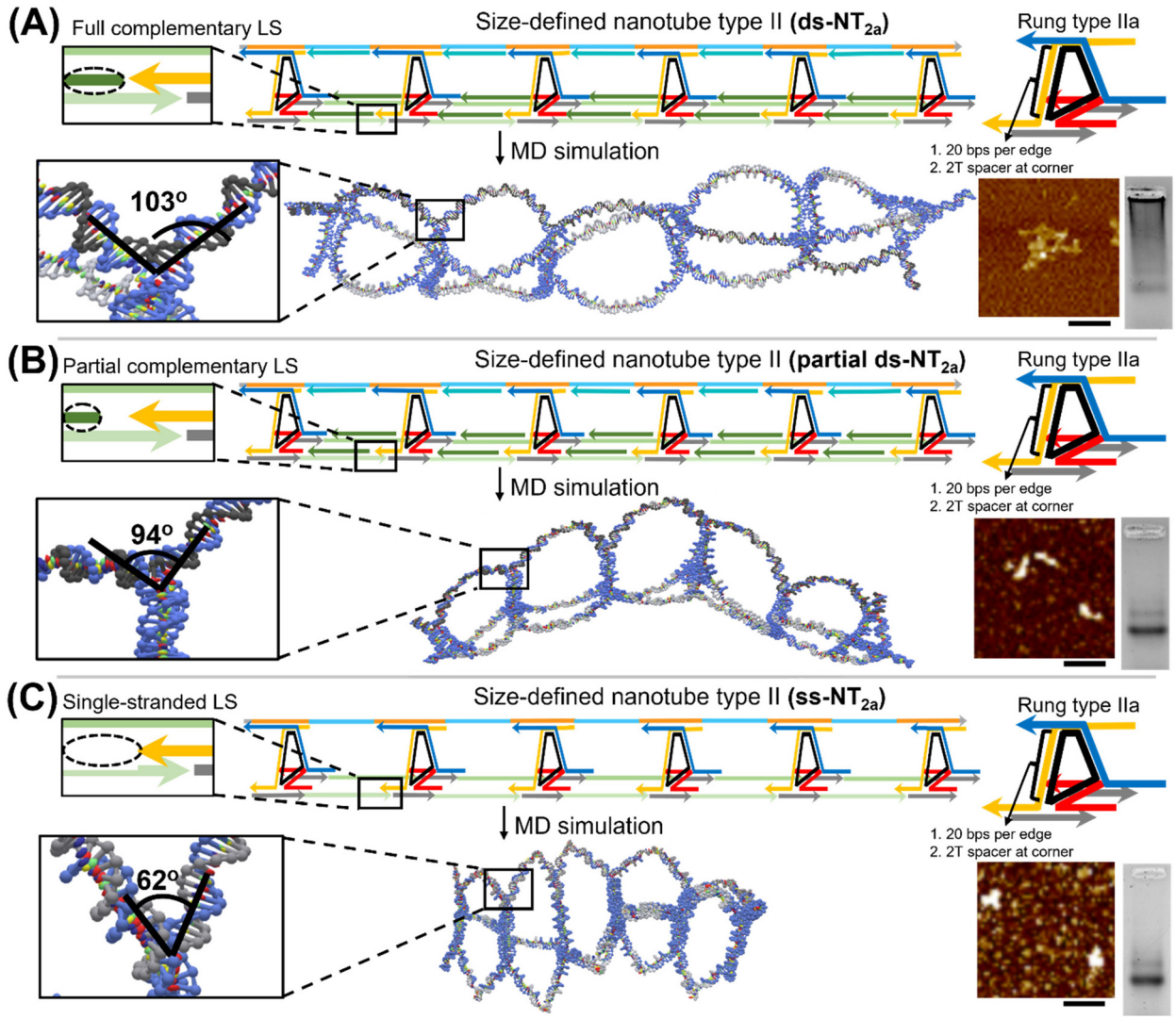

Fig. 3 Schematic representation of the fully double-stranded (ds-NT_{2a}), partially double-stranded (partial ds-NT_{2a}) and single-stranded (ss-NT_{2a}) size-defined DNA nanotube type IIa assembled using rungs with a high degree of twist. The triangular units are hybridized onto the pillar and the construction of the nanotube is completed by adding fully complementary linking strands (A), partially complementary linking strands (B) or single-stranded linking strands (C). MD simulations reveal a 103-degree, 94-degree and 62-degree angle between the rung overhangs below the triangular plane and those above the plane at the connection sites of the rungs to the pillar for ds-NT_{2a}, partial ds-NT_{2a} and ss-NT_{2a}, respectively. Small aggregates are detected by AFM for the ds-NT_{2a}, whereas partial ds-NT_{2a} and ss-NT_{2a} form collapsed structures. The scale bar is equal to 90 nm. Smearing in addition to a well-defined band are detected by AGE for ds-NT_{2a}, whereas a major well-defined band is detected for partial ds-NT_{2a} and ss-NT_{2a}.

crosslinked nanotubes (ds-NT_{2a}) along with some extended and collapsed nanotubes in the presence of fully double-stranded linking strands (Fig. 3(A)). The addition of partially double-stranded (partial ds-NT_{2a}, Fig. 3(B)) or single-stranded (ss-NT_{2a}, Fig. 3(C)) linking strands yielded collapsed structures. The extended and collapsed structures' height profiles were measured between 1.5 and 1.8 nm, indicating the stacking of some rung units within the NT_{2a}.

Another version of the fully double-stranded nanotube was successfully built using a type II rung mutant with 21 base pairs per edge and without spacers at the rung corners yielding NT_{2b}. AFM demonstrated the formation of ds-NT_{2b} with decreased flexibility (Fig. 4(A)), whereas native AGE demonstrated the formation of a discrete band with minimal smearing (Fig. 4(A)). Inserting one unhybridized base into the linking strands (Fig. 4(B)) relieves structural strain and results in a clean assembly of partial ds-NT_{2b}, but it also results in a higher degree of flexibility. Finally, when single-stranded linking strands are used in the assembly of nanotubes, collapsed structures are formed (Fig. 4(C)).

Reversible switching between partially extended and collapsed nanotubes

The dynamic nature of nanotubes enables various applications, including the encapsulation and release of cargo.[8–10] We thus investigated the structural tunability of our nanotube

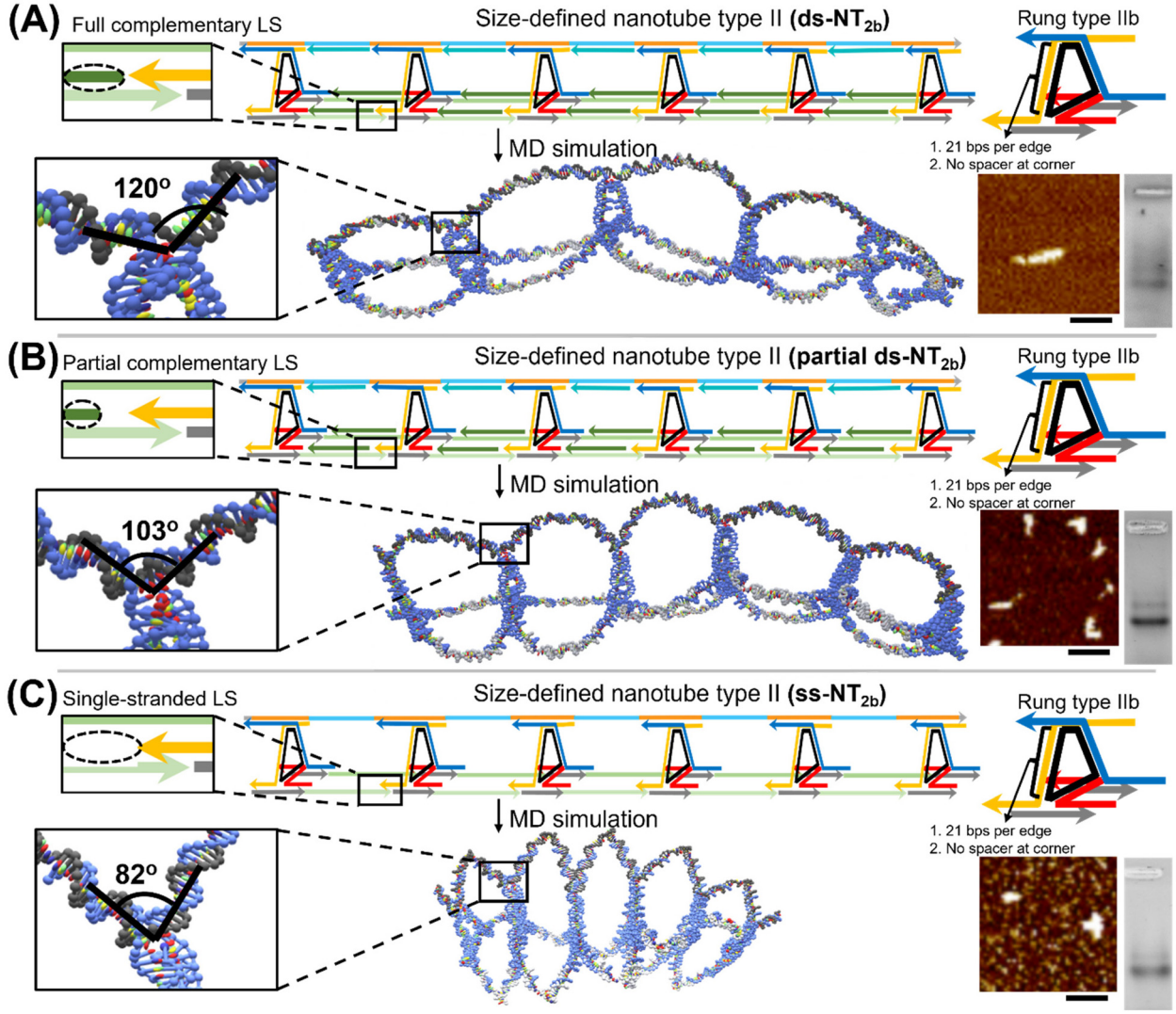

Fig. 4 Schematic representation of the fully double-stranded (ds-NT_{2b}), partially double-stranded (partial ds-NT_{2b}) and single-stranded (ss-NT_{2b}) size-defined DNA nanotube type IIb assembled using rungs with a low degree of twist. The triangular units are hybridized onto the pillar and the construction of the nanotube is completed by adding fully complementary linking strands (A), partially complementary linking strands (B) or single-stranded linking strands (C). MD simulations reveal a 12-degree, 103-degree and 82-degree angle between the rung overhangs below the triangular plane and those above the plane at the connection sites of the rungs to the pillar for ds-NT_{2b}, partial ds-NT_{2b} and ss-NT_{2b}, respectively. The scale bar is equal to 90 nm. Minor smearing in addition to a well-defined band are detected by AGE for ds-NT_{2b}, whereas a major well-defined band is detected for partial ds-NT_{2b} and ss-NT_{2b}.

by reversibly cycling between collapsed and extended configurations in response to an external stimulus. We used the toehold-mediated strand displacement technique to completely delete and refill the complementary strands of the linking (LS1 and LS2) and spacer (1a) strands.[47] We built the nanotubes using extended linking strand complements LS1/2*-ext and extended spacers 1a-ext, which have the same pattern as the original sequences but with a 10-base overhang. We next added entirely complementary strands (eraser strands), leaving the nanotube in its single-stranded form. AFM revealed collapsed structures of the fully single-stranded nanotubes (Fig. 5 (B)), while AGE showed one band with a higher mobility shift in comparison to the fully double-stranded nanotube (Fig. 5 (D), lane 4). After refilling the tube with linking strands and spacer complements, the expanded structures were regenerated (Fig. 5(C)). Native PAGE revealed a non-penetrating band with no band of higher mobility shift, indicating that the refilling was successful (Fig. 5(E)). Native AGE showed the formation of a band having a similar mobility shift as that of ds-NT_{2a} with slight smearing (Fig. 5(D), lane 2). These results are consistent with the ability of the nanotube system to cycle reversibly between extended and collapsed structures.

NT_3 – a size-defined DNA nanotube with a rigid morphology

Having formed nanotubes with collapsed and partially extended morphologies, we attempted to construct a stiff

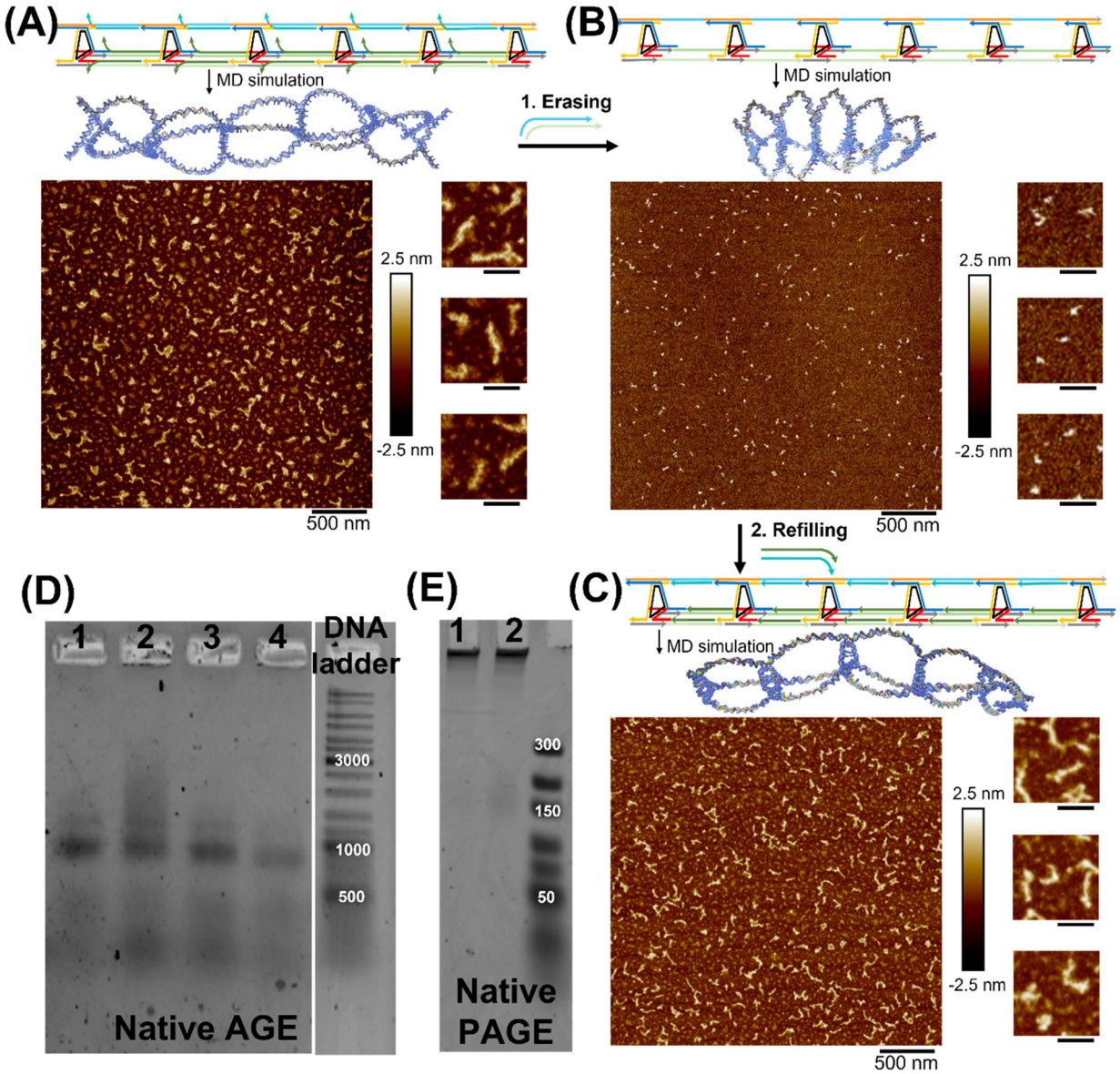

Fig. 5 Reversible switching between double-stranded and single-stranded nanotube type II (ds-NT_{2b}). ds-NT_{2a} is assembled using modified linking and spacer strands with 10-base overhangs, leading to partially extended structures readily identifiable by AFM (A). Incubation of the mixture with the fully complementary eraser strands yielded collapsed structures (B). The double-stranded form of ds-NT_{2b} is regenerated by adding a refilling strand (C). Scale bars are 500 nm and 90 nm. Native AGE characterization of ds-NT_{2b} assembled using modified linking and spacer strands with 10-base overhangs before (lane 1) and after refilling (lane 2). Incubation of the mixture with the fully complementary eraser strands yielded a product with a higher mobility shift (lane 4). Lane 3 corresponds to nanotubes formed with linking strands having no overhangs (D). Native PAGE characterization of ds-NT_{2b} assembled using modified linking and spacer strands with 10-base overhangs before (lane 1) and after refilling (lane 2) (E).

nanotube. We carefully tuned the design of the rung at the template connection site to achieve a 90° angle between the plane of the rung unit and the longwise axis of the nanotube. The right-angle formation, induced by DX tiles, eliminates the twist observed at the rung corners of previous iterations. While critical for modulating flexibility in NT_1 and NT_2, adding or removing spacers within the rung unit of NT_3 had little effect on the overall tube rigidity, as observed by MD simulations (ESI, Fig. S24†). With the inclusion of spacers, an angular twist was created between each two subsequent rung units, resulting in a total angular twist of 100° between the first and sixth rung units. The removal of these spacers yielded rigid nanotubes with no twist. MD simulations required DX tiles with a 21 bp separation between two consecutive crossover points to produce rigid nanotubes. A greater separation resulted in a substantial twist at the rung level, resulting in a flexible nanotube.

NT_3 was characterized by native AGE, revealing the formation of a well-defined band consistent with near monodispersity (Fig. 6(B)). AFM analysis demonstrated the formation of

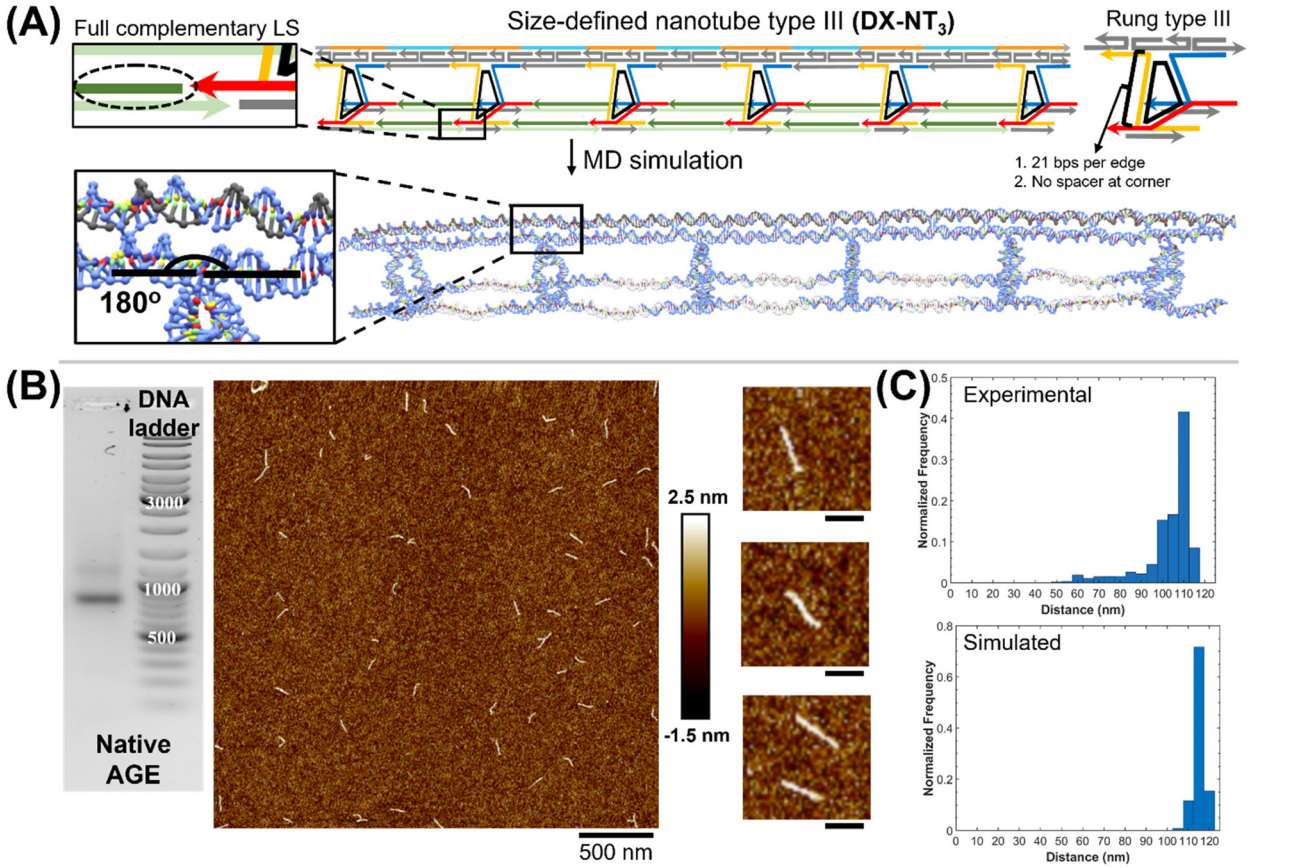

Fig. 6 Schematic representation of a size-defined DNA nanotube type III (nanotube with DX tile pillar) (DX-NT_3). Using a non-circular template, six DNA strands are thermally annealed together to generate the rung unit (rung having 21 bps per edge and the non-circular template possessing no spacers at the corner). After hybridizing the triangle units to the DX pillar, the nanotube is constructed by adding fully complementary linking strands (A). MD simulations reveal the formation of stiff tubes, with a 180-degree angle between the rung overhangs below the triangular plane and those above the plane at the connection sites of the rungs to the pillar (A), that are readily identifiable by AFM (B). AGE identifies a clean construction (B). Simulated (N = 2000, mean = 113 ± 2 nm) and experimental (N = 200, mean = 103 ± 7 nm) maximum geometric distance of DX-NT_3 (C). Scale bars are 500 nm and 90 nm.

well-defined assemblies with good rigidity and uniformity, with an average length of 103 ± 7 nm corresponding well to the expected length (115 nm) of the stiff nanotube (Fig. 6(B)).

Table 1 summarizes the experimental and simulated size distribution histograms along with the AFM and AGE data of the various NT_1, NT_{2a}, NT_{2b}, and NT_3 assemblies, revealing that the flexibility and dispersity of the nanotube assemblies can be modulated. In most cases, the experimental distribution is slightly wider than the simulated one, and the average size is slightly larger because we measured the greatest geometric distance, which may not be the exact distance between the first and last base of the main scaffold. Overall, the rung design, including the length of the rung edges and the presence of a spacer on each corner of the core template, is

Table 1 Maximum geometric distance, AFM and AGE characterization of nanotubes assembled with various rung units with different degrees of flexibility. Single-stranded linking strands yielded collapsed structures for NT_1, NT_{2a}, and NT_{2b}

LS	Characterization	NT_1	NT_{2a}	NT_{2b}	NT_3
Double-stranded LS	AFM	Aggregates	Aggregates + extended structures	Extended	Rigid
	AGE	Smear	Smear + single band	Low smear + single band	Single band
	Experimental size	NA	70 ± 21 nm	70 ± 10 nm	103 ± 7 nm
	Simulated size	79 ± 12 nm	70 ± 7 nm	70 ± 7 nm	113 ± 2 nm
Partially double-stranded LS	AFM	Collapsed	Collapsed	Partially extended	—
	AGE	Single band	Single band	Single band	—
	Experimental size	44 ± 7 nm	58 ± 9 nm	62 ± 11 nm	—
	Simulated size	47 ± 16 nm	55 ± 10 nm	59 ± 7 nm	—

a crucial parameter in determining the stiffness of the nanotube. DNA nanostructures of varying shapes and lengths have been shown to exhibit different cellular uptake and encapsulation behaviours.[44] Combining these properties with our design approach could allow an easy investigation of the cellular internalization of structures with various shapes and size.

Conclusion

In summary, we have demonstrated a simple and general method to produce DNA nanotubes with predefined lengths. This was achieved using a custom-made, long, and size-defined template strand that limits the 1D growth of the nanotubes. The template is assembled in a modular manner using a sequential growth strategy, allowing deliberate variation of its length and sequence. Nanotube formation is achieved through a two-step process involving the positioning of the pre-formed rungs onto the scaffold followed by the closure of the nanotube using linking strands. By combining experimental results and computational designs, we have examined the key parameters leading to the flexibility and rigidity of nanotubes. We found that structural flexibility about the long axis of the nanotube is directly related to the structure of the rung building blocks (*i.e.*, the cross-sectional axis). We demonstrated that some of these nanotubes are dynamic and can reversibly switch between extended and collapsed morphologies by strand displacement and subsequent rehybridization of the displaced species. Our methodology will enable ready access to deliberately constructed nanotube frameworks with user-defined stiffness and length for prospective uses in delivery applications of DNA nanostructures.

Author contributions

D. S. designed the project, contributed to the production of all experimental data, carried out most molecular dynamics and wrote the manuscript. X. L. helped in data analysis and assisted in the design of the temporal growth nanotube with a DX-tile pillar. F. J. R. helped in data analysis and co-wrote the manuscript. H. F. S. designed the project, guided the interpretation of data and result discussion, co-wrote the paper, and provided funding for the project.

Conflicts of interest

There are no conflicts to declare.

Acknowledgements

We thank the Natural Sciences and Engineering Research Council of Canada (NSERC), the Canada Research Chairs Program and the Canada Council for the Arts (Killam Fellowship) for financial support. H. F. S. is a Cottrell Scholar of the Research Corporation. F. J. R. thanks the Australia Research Council for a Discovery Early Career Research Award (DECRA).

References

1 K. E. Bujold, A. Lacroix and H. F. Sleiman, DNA nanostructures at the interface with biology, *Chem*, 2018, **4**(3), 495–521.
2 N. Liu and T. Liedl, DNA-assembled advanced plasmonic architectures, *Chem. Rev.*, 2018, **118**(6), 3032–3053.
3 J. Yin, M. Xie, J. Wang, M. Cui, D. Zhu, S. Su, C. Fan, J. Chao, Q. Li and L. Wang, Gold-Nanoparticle-Mediated Assembly of High-Order DNA Nano-Architectures, *Small*, 2022, **18**(22), 2200824.
4 J. Wang, Y. Wei, P. Zhang, Y. Wang, Q. Xia, X. Liu, S. Luo, J. Shi, J. Hu and C. Fan, Probing Heterogeneous Folding Pathways of DNA Origami Self-Assembly at the Molecular Level with Atomic Force Microscopy, *Nano Lett.*, 2022, **22**(17), 7173–7179.
5 Y. Fu, D. Zeng, J. Chao, Y. Jin, Z. Zhang, H. Liu, D. Li, H. Ma, Q. Huang and K. V. Gothelf, Single-step rapid assembly of DNA origami nanostructures for addressable nanoscale bioreactors, *J. Am. Chem. Soc.*, 2013, **135**(2), 696–702.
6 V. Linko, M. Eerikäinen and M. A. Kostiainen, A modular DNA origami-based enzyme cascade nanoreactor, *Chem. Commun.*, 2015, **51**(25), 5351–5354.
7 J. R. Burns, E. Stulz and S. Howorka, Self-assembled DNA nanopores that span lipid bilayers, *Nano Lett.*, 2013, **13**(6), 2351–2356.
8 X. Shen, Q. Jiang, J. Wang, L. Dai, G. Zou, Z.-G. Wang, W.-Q. Chen, W. Jiang and B. Ding, Visualization of the intracellular location and stability of DNA origami with a label-free fluorescent probe, *Chem. Commun.*, 2012, **48**(92), 11301–11303.
9 P. K. Lo, P. Karam, F. A. Aldaye, C. K. McLaughlin, G. D. Hamblin, G. Cosa and H. F. Sleiman, Loading and selective release of cargo in DNA nanotubes with longitudinal variation, *Nat. Chem.*, 2010, **2**(4), 319–328.
10 X. Liu, Y. Zhao, P. Liu, L. Wang, J. Lin and C. Fan, Biomimetic DNA nanotubes: nanoscale channel design and applications, *Angew. Chem., Int. Ed.*, 2019, **58**(27), 8996–9011.
11 P. Wang, S. Gaitanaros, S. Lee, M. Bathe, W. M. Shih and Y. Ke, Programming self-assembly of DNA origami honeycomb two-dimensional lattices and plasmonic metamaterials, *J. Am. Chem. Soc.*, 2016, **138**(24), 7733–7740.
12 A. Kuzyk, R. Schreiber, Z. Fan, G. Pardatscher, E.-M. Roller, A. Högele, F. C. Simmel, A. O. Govorov and T. Liedl, DNA-based self-assembly of chiral plasmonic nanostructures with tailored optical response, *Nature*, 2012, **483**(7389), 311–314.
13 R. Jungmann, M. S. Avendaño, J. B. Woehrstein, M. Dai, W. M. Shih and P. Yin, Multiplexed 3D cellular super-

resolution imaging with DNA-PAINT and Exchange-PAINT, *Nat. Methods*, 2014, **11**(3), 313–318.
14 K. Zhou, Y. Ke and Q. Wang, Selective in situ assembly of viral protein onto DNA origami, *J. Am. Chem. Soc.*, 2018, **140**(26), 8074–8077.
15 N. C. Seeman and H. F. Sleiman, DNA nanotechnology, *Nat. Rev. Mater.*, 2017, **3**(1), 1–23.
16 S. Nummelin, J. Kommeri, M. A. Kostiainen and V. Linko, Evolution of structural DNA nanotechnology, *Adv. Mater.*, 2018, **30**(24), 1703721.
17 P. Chidchob and H. F. Sleiman, Recent advances in DNA nanotechnology, *Curr. Opin. Chem. Biol.*, 2018, **46**, 63–70.
18 A. M. Maier, W. Bae, D. Schiffels, J. F. Emmerig, M. Schiff and T. Liedl, Self-assembled DNA tubes forming helices of controlled diameter and chirality, *ACS Nano*, 2017, **11**(2), 1301–1306.
19 A. Kuzuya, R. Wang, R. Sha and N. C. Seeman, Six-helix and eight-helix DNA nanotubes assembled from half-tubes, *Nano Lett.*, 2007, **7**(6), 1757–1763.
20 A. Rangnekar, K. V. Gothelf and T. H. LaBean, Design and synthesis of DNA four-helix bundles, *Nanotechnology*, 2011, **22**(23), 235601.
21 J. C. Mitchell, J. R. Harris, J. Malo, J. Bath and A. J. Turberfield, Self-assembly of chiral DNA nanotubes, *J. Am. Chem. Soc.*, 2004, **126**(50), 16342–16343.
22 P. W. Rothemund, A. Ekani-Nkodo, N. Papadakis, A. Kumar, D. K. Fygenson and E. Winfree, Design and characterization of programmable DNA nanotubes, *J. Am. Chem. Soc.*, 2004, **126**(50), 16344–16352.
23 X. Shi, X. Wu, T. Song and X. Li, Construction of DNA nanotubes with controllable diameters and patterns using hierarchical DNA sub-tiles, *Nanoscale*, 2016, **8**(31), 14785–14792.
24 P. W. Rothemund, Folding DNA to create nanoscale shapes and patterns, *Nature*, 2006, **440**(7082), 297–302.
25 J. F. Berengut, J. C. Berengut, J. P. Doye, D. Prešern, A. Kawamoto, J. Ruan, M. J. Wainwright and L. K. Lee, Design and synthesis of pleated DNA origami nanotubes with adjustable diameters, *Nucleic Acids Res.*, 2019, **47**(22), 11963–11975.
26 F. Benn, N. E. Haley, A. E. Lucas, E. Silvester, S. Helmi, R. Schreiber, J. Bath and A. J. Turberfield, Chiral DNA origami nanotubes with well-defined and addressable inside and outside surfaces, *Angew. Chem.*, 2018, **130**(26), 7813–7816.
27 B. Teshome, S. Facsko and A. Keller, Topography-controlled alignment of DNA origami nanotubes on nanopatterned surfaces, *Nanoscale*, 2014, **6**(3), 1790–1796.
28 J. F. Rahbani, E. Vengut-Climent, P. Chidchob, Y. Gidi, T. Trinh, G. Cosa and H. F. Sleiman, DNA nanotubes with hydrophobic environments: toward new platforms for guest encapsulation and cellular delivery, *Adv. Healthcare Mater.*, 2018, **7**(6), 1701049.
29 K. L. Lau, G. D. Hamblin and H. F. Sleiman, Gold Nanoparticle 3D-DNA Building Blocks: High Purity Preparation and Use for Modular Access to Nanoparticle Assemblies, *Small*, 2014, **10**(4), 660–666.
30 P. K. Lo, F. Altvater and H. F. Sleiman, Templated synthesis of DNA nanotubes with controlled, predetermined lengths, *J. Am. Chem. Soc.*, 2010, **132**(30), 10212–10214.
31 F. A. Aldaye, P. K. Lo, P. Karam, C. K. McLaughlin, G. Cosa and H. F. Sleiman, Modular construction of DNA nanotubes of tunable geometry and single-or double-stranded character, *Nat. Nanotechnol.*, 2009, **4**(6), 349–352.
32 G. D. Hamblin, A. A. Hariri, K. M. Carneiro, K. L. Lau, G. Cosa and H. F. Sleiman, Simple design for DNA nanotubes from a minimal set of unmodified strands: rapid, room-temperature assembly and readily tunable structure, *ACS Nano*, 2013, **7**(4), 3022–3028.
33 G. D. Hamblin, K. M. Carneiro, J. F. Fakhoury, K. E. Bujold and H. F. Sleiman, Rolling circle amplification-templated DNA nanotubes show increased stability and cell penetration ability, *J. Am. Chem. Soc.*, 2012, **134**(6), 2888–2891.
34 J. F. Rahbani, A. A. Hariri, G. Cosa and H. F. Sleiman, Dynamic DNA nanotubes: Reversible switching between single and double-stranded forms, and effect of base deletions, *ACS Nano*, 2015, **9**(12), 11898–11908.
35 G. D. Hamblin, J. F. Rahbani and H. F. Sleiman, Sequential growth of long DNA strands with user-defined patterns for nanostructures and scaffolds, *Nat. Commun.*, 2015, **6**(1), 1–8.
36 H. Ding, J. Li, N. Chen, X. Hu, X. Yang, L. Guo, Q. Li, X. Zuo, L. Wang and Y. Ma, DNA nanostructure-programmed like-charge attraction at the cell-membrane interface, *ACS Cent. Sci.*, 2018, **4**(10), 1344–1351.
37 X. Peng, S. Fang, B. Ji, M. Li, J. Song, L. Qiu and W. Tan, DNA Nanostructure-Programmed Cell Entry via Corner Angle-Mediated Molecular Interaction with Membrane Receptors, *Nano Lett.*, 2021, **21**(16), 6946–6951.
38 D. Jiang, Z. Ge, H.-J. Im, C. G. England, D. Ni, J. Hou, L. Zhang, C. J. Kutyreff, Y. Yan and Y. Liu, DNA origami nanostructures can exhibit preferential renal uptake and alleviate acute kidney injury, *Nat. Biomed. Eng.*, 2018, **2**(11), 865–877.
39 E. Poppleton, R. Romero, A. Mallya, L. Rovigatti and P. Šulc, OxDNA.org: a public webserver for coarse-grained simulations of DNA and RNA nanostructures, *Nucleic Acids Res.*, 2021, **49**(W1), W491–W498.
40 B. E. Snodin, F. Randisi, M. Mosayebi, P. Šulc, J. S. Schreck, F. Romano, T. E. Ouldridge, R. Tsukanov, E. Nir and A. A. Louis, Introducing improved structural properties and salt dependence into a coarse-grained model of DNA, *J. Chem. Phys.*, 2015, **142**(23), 06B613_1.
41 P. Šulc, F. Romano, T. E. Ouldridge, L. Rovigatti, J. P. Doye and A. A. Louis, Sequence-dependent thermodynamics of a coarse-grained DNA model, *J. Chem. Phys.*, 2012, **137**(13), 135101.
42 L. Rovigatti, P. Šulc, I. Z. Reguly and F. Romano, A comparison between parallelization approaches in molecular dynamics simulations on GPUs, *J. Comput. Chem.*, 2015, **36**(1), 1–8.

43 T. E. Ouldridge, A. A. Louis and J. P. Doye, Structural, mechanical, and thermodynamic properties of a coarse-grained DNA model, *J. Chem. Phys.*, 2011, **134**(8), 02B627.
44 A. Lacroix and H. F. Sleiman, DNA nanostructures: current challenges and opportunities for cellular delivery, *ACS Nano*, 2021, **15**(3), 3631–3645.
45 E. Roth, A. Glick Azaria, O. Girshevitz, A. Bitler and Y. Garini, Measuring the conformation and persistence length of single-stranded DNA using a DNA origami structure, *Nano Lett.*, 2018, **18**(11), 6703–6709.
46 D. Chakraborty, N. Hori and D. Thirumalai, Sequence-dependent three interaction site model for single-and double-stranded DNA, *J. Chem. Theory Comput.*, 2018, **14**(7), 3763–3779.
47 C. M. Platnich, A. A. Hariri, J. F. Rahbani, J. B. Gordon, H. F. Sleiman and G. Cosa, Kinetics of strand displacement and hybridization on wireframe DNA nanostructures: dissecting the roles of size, morphology, and rigidity, *ACS Nano*, 2018, **12**(12), 12836–12846.